

Remote precursor elements can modulate RNA induced silencing complex-loading efficiency of miR168 in Arabidopsis

Ágnes Dalmadi^{1,2}, Fabio Miloro^{1,2}, Auwalu Abdu^{1,2}, András Kis¹ and Zoltán Havelda^{1,2,*} 

¹Hungarian University of Agriculture and Life Sciences, Institute of Genetics and Biotechnology, Páter Károly Street 1, Gödöllő H-2100, Hungary, and

²Agribiotechnology and Precision Breeding for Food Security National Laboratory, Plant Biotechnology Section, Gödöllő H-2100, Hungary

Received 1 July 2024; revised 7 April 2025; accepted 21 April 2025.

*For correspondence (e-mail havelda.zoltan@uni-mate.hu).

SUMMARY

RNA interference mediated via the action of micro RNAs (miRNAs) plays a pivotal role in developmental and stress response pathways. In the nucleus, plant miRNAs are generated by subsequent enzymatic cuts of the *MIRNA* precursors, having specific hairpin-like secondary structures, to liberate the miRNA/miRNA* duplex. The mature miRNA strands are then loaded mostly into the ARGONAUTE 1-containing RNA induced silencing complex (RISC) with various efficiencies and trigger the down-regulation of the expression of the target mRNAs, while the miRNA* strands are eliminated. Here we revealed that *MIRNA* precursor structural elements, not overlapping with the miRNA/miRNA* duplex part, can have an influence on the AGO-loading efficiency of the produced miRNAs. Using transient and transgenic expression studies, we revealed that a chimeric *MIR168* precursor hairpin structure containing the stem region of a *hvu-MIR171* precursor can induce the enhancement of AGO-loading efficiency of the produced miR168, resulting in increased target down-regulation and in developmental defects of the transgenic plants. This effect was the most pronounced when the orientation of the wild-type miR168/miR168* duplex was inverted in the chimeric precursor, implying the cooperative action of the structural elements. In transient studies, we also showed that precursor elements of *MIR168a* can reduce AGO-loading efficiency of miR171. The discovery of signals on remote structures of the miRNA precursor suggests that miRNA biogenesis and AGO-loading can be spatially more connected in the nucleus and/or signalization events mediated by these non-duplex structural features during miRNA biogenesis can determine the fate of the miRNA/miRNA* duplexes in separated AGO-loading processes.

Keywords: RNA interference, miRNA precursor structure, AGO1, loading efficiency, miR168, miRNA biogenesis.

INTRODUCTION

The action of RNA interference (RNAi) via the activity of micro RNAs (miRNAs) is a widely spread regulatory mechanism of gene expression both in animal and in plant systems (Carrington & Ambros, 2003). This highly conserved pathway affects a series of developmental processes and also abiotic or biotic stress responses (Dong et al., 2022; Sunkar et al., 2012).

In plants, miRNAs originate from RNA Polymerase II (Pol II) transcribed precursor RNA molecules (pri-miRNAs) having a specific hairpin-like secondary structure. Pri-miRNAs are capped and polyadenylated, then processed at the hairpin structure typically by DICER LIKE 1 (DCL1) to generate pre-miRNA intermediates and subsequently 20–24 nucleotide

(nt) long double-stranded miRNA/miRNA* duplexes. The processing of pri-miRNAs requires co-factors such as the zinc finger protein SERRATE (SE) and the dsRNA-binding domain protein HYPOASTIC LEAVES1/DOUBLE-STRANDED RNA-BINDING PROTEIN 1 (HYL1/DRB1) (Ding & Zhang, 2023; Li & Yu, 2021). The miRNA/miRNA* duplexes are methylated by the sRNA methyltransferase HUA Enhancer 1 (HEN1) at the 3' ends to aid their protection against exonucleases (Xu & Chen, 2023).

The main executor molecules of RNAi are the ARGONAUTE (AGO) proteins, which are specialized in diverse pathways but often show redundancies in their action. The mature miRNA strand of miRNA/miRNA* duplexes is typically loaded into AGO1 protein containing RNA-induced

silencing complexes (RISCs) while the miRNA* strands are eliminated (Mallory & Vaucheret, 2010). As the main executor component of miRNA-mediated regulatory actions, the expression of AGO1 is tightly regulated at post-transcriptional (Vaucheret et al., 2006) and post-translational (Hacquard et al., 2022) levels to avoid the deteriorating effects of the loading of illegitimate small RNAs. The miRNA-loaded RISCs are directed to the target mRNA molecules in a sequence-specific manner, triggering their negative regulation via cleavage or translational inhibition (Ding & Zhang, 2023; Li & Yu, 2021; Mencia et al., 2023).

Several common enzyme participants and processes of miRNA biogenesis and action were identified in plants and animals (Axtell et al., 2011). Structural features of the miRNA precursor hairpins were proven to be pivotal regulators of the biogenesis of miRNAs (Xu & Chen, 2023). The size and shape of plant miRNA precursors are very variable, but despite this diversity, they accurately produce the various miRNAs (Bologna et al., 2013; Moro et al., 2018). Precursors which possess 15–17 base-pair (bp) double-stranded (ds)RNA segments at the base of the miRNA/miRNA* duplex are processed in a base-to-loop manner, where the first cleavage of DCL1 is at the proximal part of the miRNA duplex (Mateos et al., 2010; Song et al., 2010; Zhu et al., 2013). Another group of miRNA precursors possesses the dsRNA segment above the miRNA/miRNA* duplex, and the first DCL1 cut releases the terminal loop, resulting in loop-to-base processing (Addo-Quaye et al., 2009; Bologna et al., 2009; Moro et al., 2018). In plants, after the first cut, DCL1 also produces the subsequent cleavage typically at a 21 nt distance, liberating the miRNA/miRNA* duplex. Both cleavage steps are thought to take place in the nucleus (Mencia et al., 2023).

Alterations in the miRNA precursor hairpin structure can induce the mis- or reduced production of mature miRNAs (Mateos et al., 2010; Song et al., 2010; Werner et al., 2010). It was also shown that specifically located sequence biases are present in plant miRNA primary transcripts affecting miRNA biogenesis (Narjala et al., 2020; Rojas et al., 2020). The released miRNA/miRNA* duplex itself also contains sequence and structural motifs regulating subsequent processes (Iki, 2017). The active miRNA strand is selected according to the thermodynamic stability of the miRNA duplex ends (Eamens et al., 2009), and the 5'-nucleotide strongly determines the AGO sorting capabilities of the mature miRNAs (Mi et al., 2008; Takeda et al., 2008). miRNAs specific for AGO1 loading typically have uridine at their 5' end (5' U) (Mi et al., 2008). Structural features located on miR165/miR165*, miR166/miR166*, and miR390/miR390* duplexes select them specifically to be associated with AGO10 and AGO7, respectively (Endo et al., 2013; Zhu et al., 2011). Modifications of miRNA/miRNA* duplexes in transient expression

studies showed that structural motifs can control AGO1 and/or AGO2 sorting (Zhang et al., 2014).

AGO1 expression is also regulated through RNAi via the self-regulatory action employing miR168 (Mallory & Vaucheret, 2010). It was also shown that the sorting of miR168 into AGO1 or AGO10 is controlled by metastable structural configurations of the *MIR168* precursor favoring the production of 22 nt miR168 species (Iki et al., 2018).

Recent studies revealed that besides biogenesis and sorting, structural features of the miR168/miR168* duplex can also affect the loading efficiency of miR168 into AGO1 (Dalmadi et al., 2021). This new regulatory layer, controlling AGO1 loading efficiency of miRNAs, was discovered by utilizing size-separating gel-filtration experiments that identified AGO1-bound and AGO-unbound miRNA pools. It was demonstrated that miRNAs were typically associated with AGO1-containing high molecular weight RISCs (HMW-RISCs) but a large set of cytoplasmic miRNA species, most likely miRNA/miRNA* duplexes, were also identified at the low molecular size range corresponding to AGO-unbound miRNAs. In-depth investigation of the HMW-RISC co-localized and the AGO-unbound pool composing miRNA sequences revealed large differences in AGO-loading efficiencies of various miRNAs, ranking them into low, moderate, and high AGO-loading classes. The loading properties of miRNAs belonging to different AGO-loading classes remained invariable under the over-expression of their precursor fragments, as the over-expressed miRNAs showed similar distribution patterns between the HMW-RISC and AGO-unbound pools as were experienced in wild-type plants, indicating that not the abundance of the particular miRNAs but rather their precursor features determine the AGO-loading capabilities (Dalmadi et al., 2019).

It was shown that the *AGO1* mRNA targeting miR168 belongs to the low AGO-loading class and accumulates predominantly in the AGO-unbound cytosolic pool. However, modification of the miR168/miR168* duplex structure inside the *MIR168a* precursor fragment can alter the finely adjusted loading efficiency of miR168 (Dalmadi et al., 2021). In addition, the expression of miR168 from the artificial (a)*MIR171*-based precursor fragment, which miRNA exhibits high AGO-loading capacity, can also alter the finely adjusted loading efficiency of miR168 (Dalmadi et al., 2021). In these experiments, the miR168* strands were modified in such a way that the miR168/modified-miR168* duplexes mimicked the structural properties of the miR171/miR171* duplex. Based on these data, the observed AGO-loading differences were mainly attributed to structural features of the miRNA/modified-miR168* duplex. It remained unclear whether structural or sequence elements of the precursor bordering the miRNA/miRNA* duplex can take part in the regulation of miRNA loading efficiency.

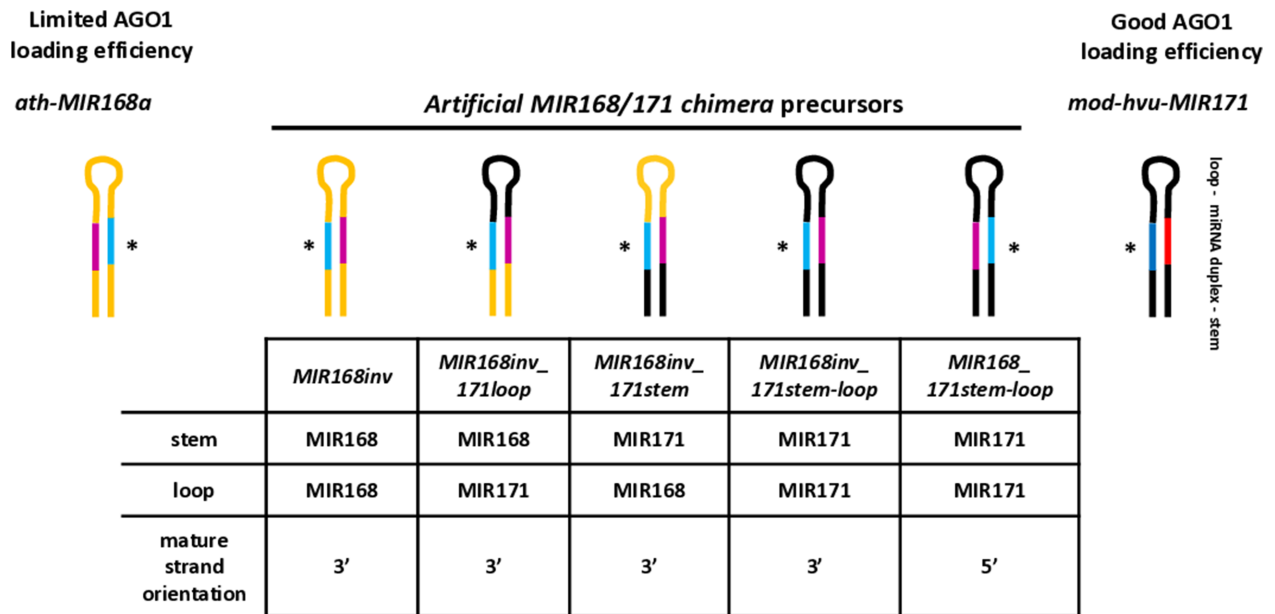


Figure 1. Schematic representation of the wild-type *ath-MIR168a*, the *hvu-MIR171* based, and the used artificial chimeric miR168 producing precursor fragment constructs.

Pink and red show mature miR168 and miR171, respectively; light blue and dark blue highlight the corresponding star strands. Yellow and black lines represent the respective *ath-MIR168* and modified *hvu-MIR171* precursor parts. The composition of the chimeric precursor fragments is presented in the table below. Asterisks label the miR168 passenger strands within the constructs. * the miR168 passenger strands within the constructs.

Here we show that maturation of the canonical miR168/miR168* duplex from different precursor backbones can alter the loading efficiency of miR168, inducing enhanced target down-regulation. We show that replacement of the proximal stem part of *MIR168a* precursor with the corresponding segment of *hvu-MIR171* precursor, which exhibits more efficient AGO-loading properties, together with the inversion of the duplex region, increases the AGO-loading of miR168. These findings imply that in addition to the signals on the miR168/miR168* duplex, remote non-duplex parts of the precursor could also take part directly or indirectly in the regulation of AGO-loading efficiency of miR168.

RESULTS

Generation of *MIR168/MIR171* chimeric precursor constructs encompassing the canonical miR168/miR168* duplex

To investigate the effect of *MIRNA* precursor backbone elements, flanking the miR168/miR168* duplex region, on the AGO1 loading efficiency and target down-regulation ability of miR168, five artificial chimeric (a)*MIR168* precursor constructs were built. The proximal (stem) and the distal (loop) regions of *ath-MIR168a* producing the low AGO1-loading miR168 (Dalmadi et al., 2019, 2021) were replaced by components of the more efficiently AGO1-loaded *MIR171* precursor fragment using the modified barley *hvu-MIR171* precursor described previously (Kis et al., 2016) (Figure 1).

Since *MIR168a* and *hvu-MIR171* precursors differ not only in their backbone sequence and structure but also in the orientation of the miRNA/miRNA* duplexes, as the mature miRNAs originate from opposite arms of the hairpin structure, the role of the miRNA duplex orientation was also investigated. First, to test the effect of the orientation alone the miR168/miR168* duplex region was inverted in the original *MIR168a* precursor resulting in the *MIR168inv* construct so that the mature strand was situated on the 3' arm of the hairpin structure similarly to *hvu-MIR171* precursor (Figure 1; Figure S1). Next, retaining the inverted miR168 duplex orientation, three additional constructs were built by replacing *MIR168a* backbone parts with *hvu-MIR171* elements. Replacement of the distal (loop) or the proximal (stem) precursor parts generated *MIR168inv_171loop* and *MIR168inv_171stem* chimeric constructs, respectively. Substituting both proximal and distal elements produced the *MIR168inv_171stem-loop* chimeric construct (Figure 1). A similar construct was also built, containing the original 5' arm mature strand orientation of the miR168/miR168* duplex (*MIR168_171stem-loop*) (Figure 1). Thus, *MIR168inv_171stem-loop* and *MIR168_171stem-loop* chimeric constructs differ only in the orientation of the mature miR168. All five modified precursor constructs were designed to retain the intact mature miR168 sequence allowing the production of the wild-type active form of miR168. In all cases, the structure of the miRNA duplexes and the sequence of the miR168* region corresponding to the mature miRNA remained identical to wild-type

structure and sequences. The two-nucleotide overhang of the miR168* strand or the backbone nucleotides pairing with the overhangs were adjusted solely to retain the original RNA secondary structure at the duplex-backbone junctions (Figure S1).

Chimeric precursors exhibit various target down-regulation efficiencies in transient assay

The modified precursor constructs were tested for their target down-regulation properties in transient assays utilizing *Agrobacterium* infiltration of young *Nicotiana benthamiana* leaves. To visualize the effect of miR168 over-expression, a previously built AGO1-sensor construct was co-infiltrated with the miRNA precursor constructs (Dalmadi et al., 2021). This sensor contained a 558 bp fragment of the *AGO1* gene with the miRNA target site inside fused to the *GFP* reporter gene in frame. The AGO1-sensor construct was used in the same concentration for every *Agrobacterium* suspension mixture, which also contained the same amount of viral P14 suppressor expressing binary construct to prevent the establishment of transgene-induced siRNA-mediated RNAi. All the constructs used in this study were under the control of the constitutive 35S promoter but produced various amounts of mature miR168 when applied in the same concentration of bacteria in infiltration experiments (Figure S7e). To focus on the target down-regulation properties of the produced miR168, the concentration of the chimeric precursor constructs was adjusted to produce miR168 at a comparable level to the control wild-type *MIR168a* precursor (Figure 2b). Since the *MIR168_171stem-loop* construct consistently produced a lower level of miR168, we diluted proportionally the *MIR168a* construct to ensure comparability in its assays (Table S1). Minimizing the alterations occurring between leaves at different developmental stages, the two sides of the individual leaves were used to infiltrate the various modified constructs in parallel with the wild type *MIR168a* precursor fragment construct. Replica samples were then collected in parallel, each bulked from four leaves, and every experiment was repeated 3–5 times. Relative signal intensities of AGO1-sensor protein were calculated on the basis of the corresponding control *MIR168a* infiltrated samples and were subjected to statistical analysis (Table S2). Changing the orientation of the miR168/miR168* duplex in its own precursor backbone (*MIR168inv*) had a marginal effect on GFP signal and consequently on AGO-sensor protein level (Figure 2a,b; Figure S2). The addition of *hvu-MIR171* originated loop to the inverted miR168 duplex, resulting in the *MIR168inv_171loop* chimeric precursor fragment, did not prove to be sufficient to induce significantly elevated target down-regulation. The observed small-scale tendency of AGO1-sensor protein signal loss (Figure 2a,b; Figure S3) was not significant compared with the wild-type *MIR168a* precursor (Figure 2c). In contrast,

the replacement of the proximal part of the *MIR168inv* hairpin structure with *hvu-MIR171* stem structure (*MIR168inv_171stem*) resulted in the significant reduction of the visible GFP signal alongside the sensor protein level (Figure 2a–c; Figure S4). This effect was slightly more pronounced when both the stem and the loop sections of the *MIR168inv* precursor were replaced by the *hvu-MIR171* originated stem and loop regions, resulting in the *MIR168inv_171stem-loop* construct (Figure 2a–c; Figure S5). Intriguingly, restoring the miR168 duplex orientation back to the orientation of the wild-type *MIR168a* precursor in *MIR168_171stem-loop*, where mature miR168 is originated from the 5' side of the hairpin structure, decreased the efficiency of GFP sensor down-regulation. The AGO1-sensor level showed only a moderately higher down-regulation effect compared with *MIR168a* control infiltration with a relatively high variance in the observed protein signal intensity (Figure 2a–c; Figure S6). Taking all together, at a similar level of miR168 production, the target inhibitory action was significantly enhanced when the orientation of the natural miR168 duplex was inverted and the flanking proximal structural element was replaced by the *hvu-MIR171* stem. These data indicate that sequence and/or structural elements of the miR168/miR168* duplex bordering regions of the precursor RNA can significantly affect the action of miR168, possibly at the level of RISC-loading.

Transiently over-expressed chimeric precursors show increased miR168 HMW-RISC loading

It was shown previously that the target down-regulation ability of miR168 is in strong connection to its HMW-RISC-loading efficiency (Dalmadi et al., 2021). To monitor the presumed changes in miR168 HMW-RISC-loading efficiency of the different chimeric precursors, gel-filtration experiments were carried out as described previously, using crude extracts from *N. benthamiana* leaves transiently over-expressing the precursor constructs (Dalmadi et al., 2019, 2021). To avoid the oversaturation of the signals, short exposures of the northern blots were presented and used for the calculation of loading efficiencies. Under these circumstances, *MIR168a* derived miR168 was not detected in HMW-RISC and became visible only after applying long exposure time. In line with previous observations, we found that transient expression of the *MIR168a* precursor fragment resulted in the massive accumulation of the unbound miR168 pool, and only a minor miR168 subset was present in HMW-RISC (Figure 2d; Figure S7a,c). Over-expression of *MIR168inv* was associated with a slight increase, below the significance, in the level of HMW-RISC bound miR168 compared with *MIR168a*. Exchanging the loop region of *MIR168inv* for the *MIR171* loop in *MIR168inv_171loop* moderately further increased the level of HMW-RISC bound miR168. In contrast, transient

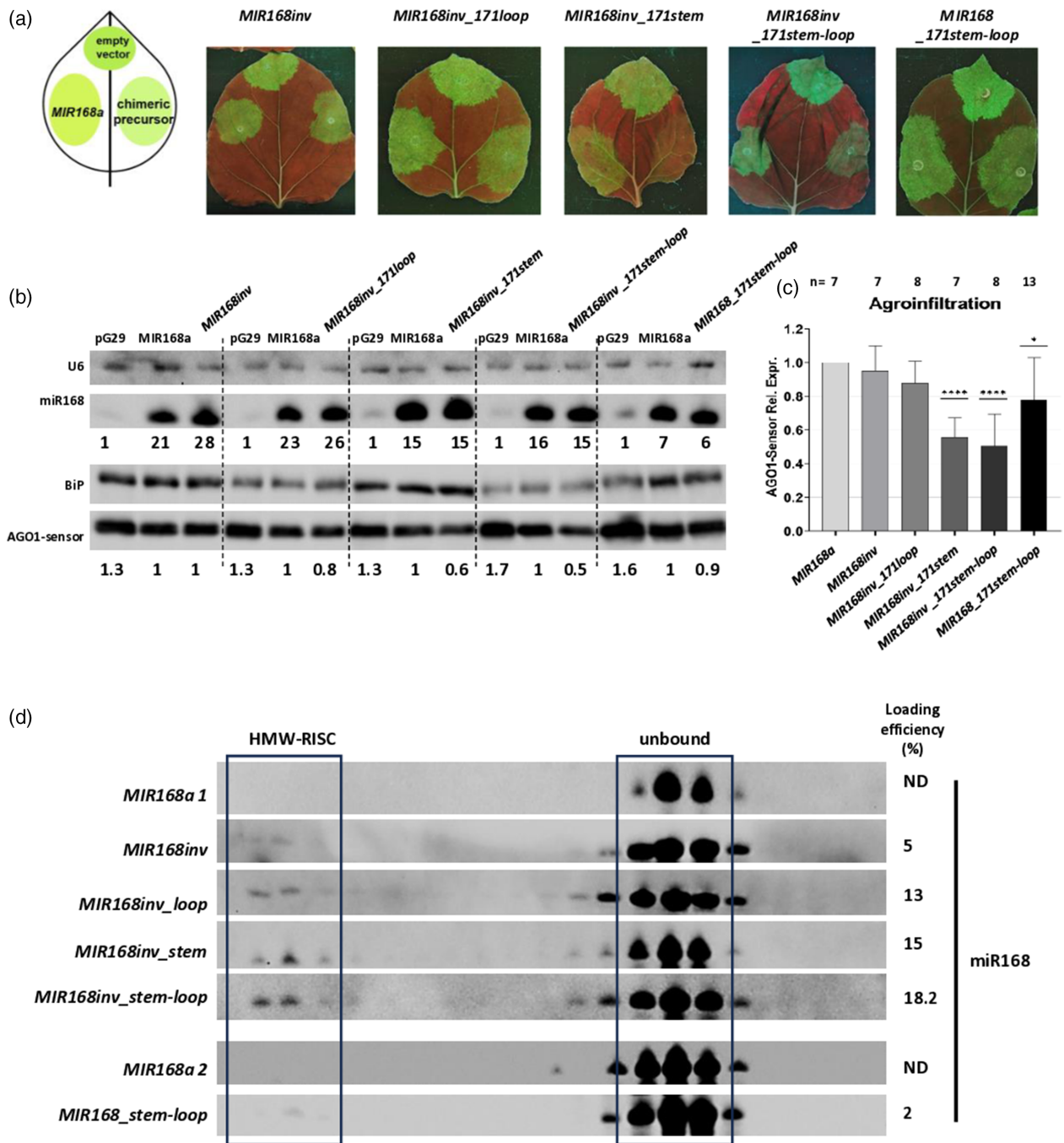


Figure 2. Transient assay of the manipulated miR168 producing precursor constructs.

(a) GFP signal of *N. benthamiana* leaves infiltrated with *Agrobacterium* mixture of AGO1-sensor, P14 viral suppressor of the siRNA pathway, and pGreen0029 empty vector on leaf edge, *MIR168a* on left side, or the different chimeric precursor constructs on the right side. For detailed composition of *Agrobacterium* mixtures, see Table S1.

(b) MiR168 and AGO1-sensor accumulation in infiltrated leaf patches. U6 and BiP were used as a loading controls on RNA and protein levels, respectively. MiR168 and AGO1-sensor signals were normalized to U6 and BiP, respectively, and changes relative to *MIR168a* infiltration of the corresponding experiment were displayed.

(c) Statistical evaluation of multiple experimental results between *MIR168a* and each manipulated precursor construct in terms of AGO1-sensor down-regulation. Relative volume intensity of AGO1-sensor protein was normalized to BiP and presented on the basis of the signal observed with *MIR168a*. Significant differences in comparison with *MIR168a* were indicated with asterisks. (ANOVA one-way with Dunnett's post-hoc test, * <0.05 , and **** <0.0001).

(d) MiR168 distribution amongst gel-filtration fractions prepared from the infiltration of the used precursor constructs. To allow comparison of lower over-expressor *MIR168_stem-loop*, *MIR168a* construct was infiltrated also in a lower concentration (*MIR168a 2*). Loading efficiency was calculated based on the summarized volume intensities and as $\text{HMW-RISC}/(\text{HMW-RISC} + \text{unbound}) \times 100$.

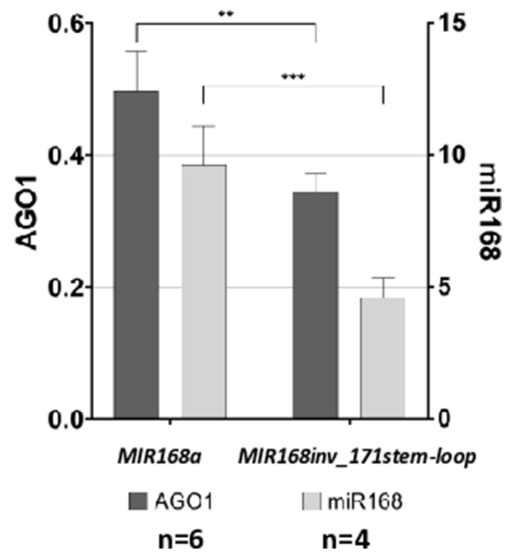
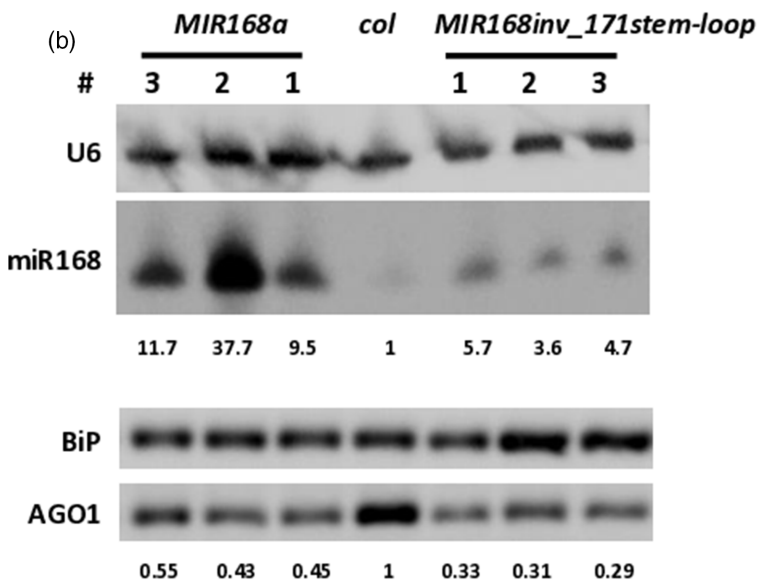
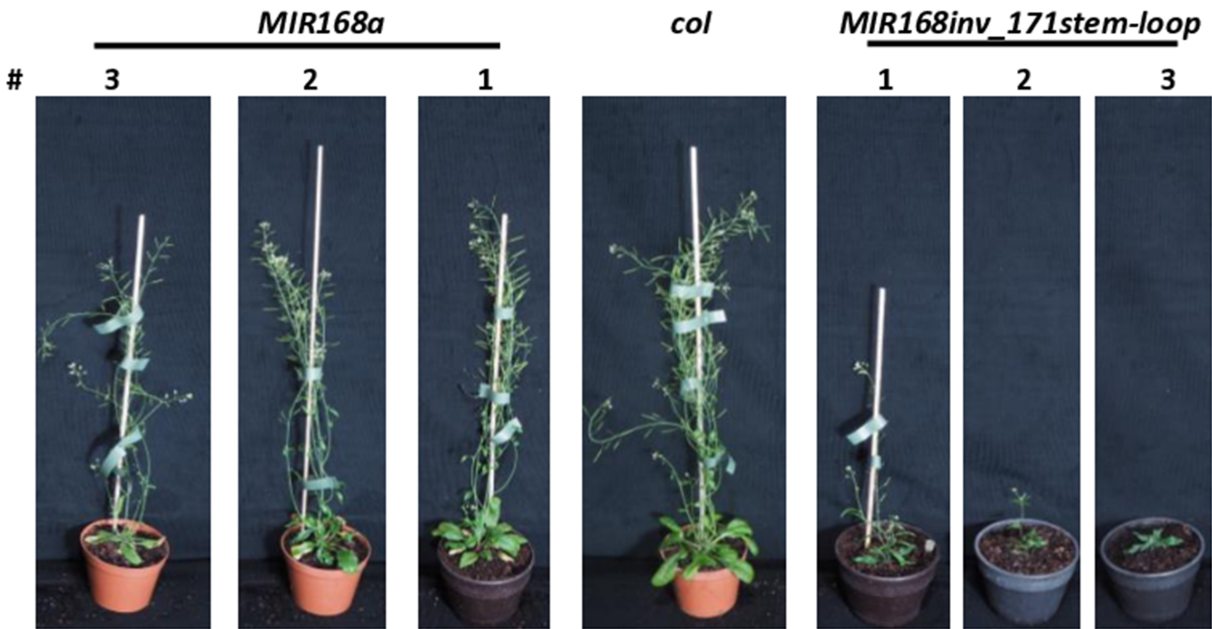
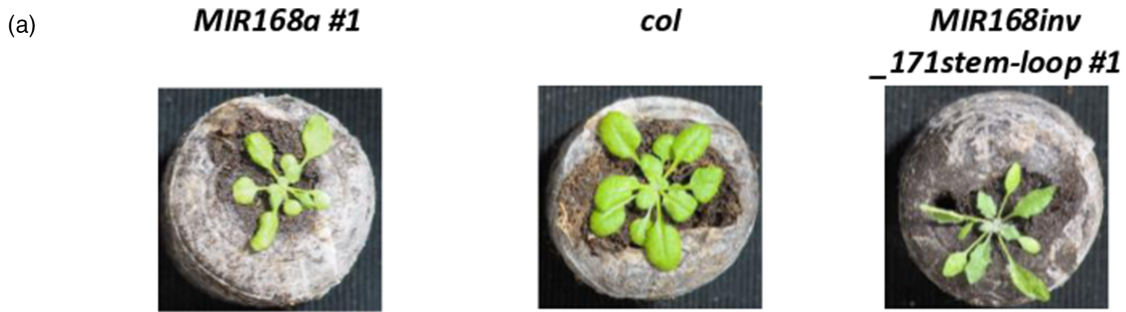


Figure 3. Phenotypical and molecular characterization of *MIR168inv_171stem-loop* transgenic plants.

(a) Rosettes and general phenotype of 6- and 11-week-old *MIR168a* and *MIR168inv_171stem-loop* precursor fragment over-expressing transgenic plants. (b) miR168 and AGO1 accumulation in representative over-expressing transgenic lines of *MIR168a* and *MIR168inv_stem-loop* precursor constructs. U6 and BiP serve as RNA and protein internal controls, respectively. Graph shows statistics of six and four *MIR168a* and *MIR168inv_stem-loop* transgenic lines selected based on their close over-expression rate (between 3 and 12 times compared to *Columbia* wild type). (ANOVA one-way with Dunnett's post-hoc test, **<0.01, and ***<0.001).

expression of *MIR168inv_171stem* and especially *MIR168inv_171stem-loop* chimeric precursors induced a more pronounced accumulation of miR168 in HMW-RISC (Figure 2d; Figure S7c). This enhanced loading efficiency was mostly eliminated by reinverting the orientation of the miR168 duplex in the chimeric construct *MIR168_171stem-loop* (Figure 2d; Figure S7c). The presence of functional HMW-RISC in the conducted experiments was demonstrated by the detection of the high HMW-RISC-loading type miR159 (Dalmadi et al., 2019) (Figure S7b). According to our data, all modifications of the miRNA precursor structure/sequence resulted in the elevation of miR168 HMW-RISC-loading efficiency, but with various extents (Figure 2d; Figure S7c). The enhanced miR168 HMW-RISC-loading properties correlated with the abilities of the various chimeric precursors to down-regulate the AGO-sensor construct (Figure 2a–c). The highest miR168 HMW-RISC-loading efficiency was detected in the cases of *MIR168inv_171stem* and *MIR168inv_171stem-loop*. Our data indicate that the stem part of the miRNA precursor structure, in cooperation with the inverted miR168/miR168* duplex structure, plays a pivotal role in the determination of the AGO-loading ability of the generated miR168 species.

Transgenic over-expression of *MIR168inv_171stem-loop* precursor fragment construct enhances miR168 activity

Since *MIR168inv_171stem-loop* chimeric precursor fragment construct was identified to have the highest target down-regulation capacity amongst the chimeric constructs, this was used to produce transgenic over-expressor lines in *Arabidopsis thaliana*. To assess the target down-regulation capability of this chimeric precursor, wild-type *MIR168a* precursor fragment was also used to create transgenic plants expressing miR168 with different extents. Transgenic lines over-expressing *MIR168inv_171stem-loop* precursor fragment exhibited more pronounced phenotypic alterations compared with their *MIR168a* over-expressing counterparts exhibiting even higher miR168 content (Figure 3a; Figure S8a). In consistency with former studies (Dalmadi et al., 2021; Vaucheret et al., 2006), the moderate over-expression of the wild-type *MIR168a* precursor fragment was associated with mild phenotypical alterations, like serrated leaves and slightly delayed flowering. *MIR168inv_171stem-loop* transgenic plants exhibited more severe developmental alterations resembling more *ago1* genetic mutants (Morel et al., 2002) with elongated leaf petioles, pointed oval curled, and serrated leaves and a darker

green color. At the age of 11 weeks, plants over-expressing the chimeric precursor were stunted with less and delayed flowering stems compared with *MIR168a* transgenic plants (Figure 3a; Figure S8a). The more severe phenotype was also associated with reduced seed production. The molecular characterization of the over-expressor plants revealed that the lower level of miR168 production derived from the *MIR168inv_171stem-loop* chimeric precursor fragment was significantly more effective in down-regulation of AGO1 protein level than the higher level of miR168 originated from *MIR168a* precursor (Figure 3b; Figure S8b). To reveal whether the observed increase in target down-regulation was due to the higher representation of miR168 in AGO1 containing HMW-RISC pool, a gel-filtration experiment was carried out using one medium miR168 over-expressor *MIR168a* transgenic line and the *MIR168inv_171stem-loop* line showing the highest miR168 content. A sub-portion of the crude extract used in the gel-filtration experiment was used to demonstrate miR168 and AGO1 content of the input samples. The selected *MIR168a* control line exhibited higher miR168 content than the used *MIR168inv_171stem-loop* line (Figure S9). Gel-filtration fractions were divided into two series; fractions with odd numbers were used to investigate miR168 distribution while even number fractions were used for western blotting to identify AGO1 protein as described previously (Dalmadi et al., 2019). To enable the comparison, northern blots were developed to show similar volume intensities in fractions representing the unbound miR168 pool. Loading efficiency was calculated from cumulative intensities of the 3–3 most prominent HMW-RISC and unbound pool signals, and the first was referred to the sum of the two volume intensities (HMW-RISC/(HMW-RISC+unbound)). The relative loading efficiency took the total AGO1 level also into consideration. The moderate over-expressor *MIR168inv_171stem-loop* line showed similar miR168 signal intensities in HMW-RISC fractions as the *MIR168a* line despite the presence of only half AGO1 content in the corresponding fractions (Figure S9). This observation suggests that miR168 species produced by *MIR168inv_171stem-loop* fragment in the *Arabidopsis* plants exhibit a more efficient loading capacity into AGO1 containing HMW-RISC.

Processing of *MIR168inv_171stem-loop* precursor generates canonical miR168 species

Despite our intention to retain the original miR168 production, our experimental setup could raise the question

of whether the over-production of miR168 from the chimeric precursor fragment induced the misprocessing of the miR168/miR168* duplex, generating various non-canonical miR168 species that can lead to the misinterpretation of the data. To assess this possibility and to acquire comprehensive data on miR168 species matured in the stable transgenic lines, high-throughput sequencing (HTS) analyses of sRNA pools of *MIR168a* and *MIR168inv_171stem-loop* transgenic plants were carried out. RNA samples of seedlings originating from the representative lines were used for HTS in two replica experiments. Following the quality check, adapter and stop oligo sequence trimming of the HTS data, reads between 15 and 30 nt were mapped onto the mature strand containing arm of the corresponding miR168 producer precursor sequences and were analyzed for their size distribution percentage and quantity (Figure 4a). In line with the northern blot data, the reads per million (RPM) values of reads mapped onto the precursors were significantly less in *MIR168inv_171stem-loop* transgenic plants than in *MIR168a* over-expressing plants (Figure 4a). In the case of both constructs, the 20–22 nt long sRNA species exhibited the highest abundance with 85–87% and 92–93% for *MIR168a* and *MIR168inv_171stem-loop*, respectively. The HTS data revealed that the over-expression of the *MIR168inv_171stem-loop* precursor fragment construct was associated with a moderately higher percentage of 20 nt sRNA species compared with *MIR168a*. Based on the similar analyses of previous sequencing data (Mi et al., 2008), the 20 nt long miR168 species, similarly to the 21 nt long ones, are also AGO1-loading competent, indicating that they are biologically active (Figure S10). The HTS reads mapped to the mature strand containing arm of the hairpin were further investigated for their 5' end nucleotide identity. No changes in the distribution among the categories were detected as, in both cases, about 90% of the reads had an uracil and 6–9% a cytosine at their 5' terminus (Figure 4b). Comparing the 10 most abundant iso-miRs of the data sets revealed that in all cases the classical miR168 species were over-represented (Figure 4c) suggesting unaltered AGO1 sorting capabilities of the generated miRNAs. To check whether non-canonical processing of the chimeric precursor could result in some non-classical miRNA/miRNA* duplexes, we also analyzed the reads corresponding to the miR168* strands. We found the 21 nt long classical miR168* strand to be over-represented in all cases (Table S3). HTS data were also used to investigate the *AGO1* mRNA originated siRNAs, as well. Based on the analyses of *AGO1* mRNA specific siRNAs, no significant difference was detected between *MIR168a* and *MIR168inv_171stem-loop* (Figure S11). AGO1 sorting of miR168 in *MIR168a* and *MIR168inv_171stem-loop*

transgenic plants was also confirmed in the AGO1 immuno-precipitation experiment (Figure S9b).

Distant precursor elements affect the AGO-loading efficiency of miR171 in collaboration with duplex features in transient assay

To further test the relative contribution of precursor elements to the determination of the loading efficiency of the produced miRNA, additional artificial and/or chimeric precursor constructs involving the elements of *ath-MIR168a* were created. In this experiment, the barley-originated miR171 was tested for how its precursor features contribute to the originally high loading capacity. All the created constructs contained the wild type miR171, which was produced from the backbone either of *MIR168a* or *hvu-MIR171*, with the original or a modified star/passenger strand (Figure 5a; Figure S12). Firstly, wild-type miR171/miR171* duplex was inserted in the *MIR168a* backbone either with 5' or with 3' mature strand orientation, producing the *MIR171inv_168stem-loop* and *MIR171_168stem-loop* constructs. To test the combined effect of duplex structure and remote precursor elements, constructs mimicking miR168/miR168* duplex structure in either *MIR168* or *hvu-MIR171* backbone were built (*MIR171invstar* and *aMIR171*). The precursor constructs were tested for their ability to produce miR171 in a transient assay (Figure S7f; Table S1), and the transiently produced miR171 was investigated with gel-filtration to observe the loading efficiency (Figure 5b; Figure S13). Functional high molecular weight RISCs were detected using the highly loaded miR159 (Figure S7d). The similar distribution pattern of miR171 expressed from *ath-MIR171a* and the modified *hvu-MIR171* demonstrates the conserved nature of the loading efficiency. Changes in the remote precursor parts alone in the case of *MIR171inv_168stem-loop* caused a moderate but obvious decline in the loading efficiency of miR171, showing a shift from high molecular weight AGO complexes to the fractions corresponding to the non-complexed AGO proteins (Figure 5b). This effect becomes more pronounced when the miR171/miR171* duplex orientation corresponds to the *hvu-MIR171* precursor in the *MIR168a* backbone, in *MIR171_168stem-loop*. In this case, we observed the enhanced accumulation of unbound miR171 species, indicating the cooperative action of various precursor elements. The modification of the passenger strand to mimic miR168/miR168* structure and using inverted duplex orientation together in *hvu-MIR171* backbone itself resulted in a remarkable loss in the loading efficiency. This observation highlights the pivotal role of the miRNA duplex properties in determining AGO loading. Moreover, the further reduction of high molecular weight AGO-bound miR171 and the aggravated presence of unbound miRNA

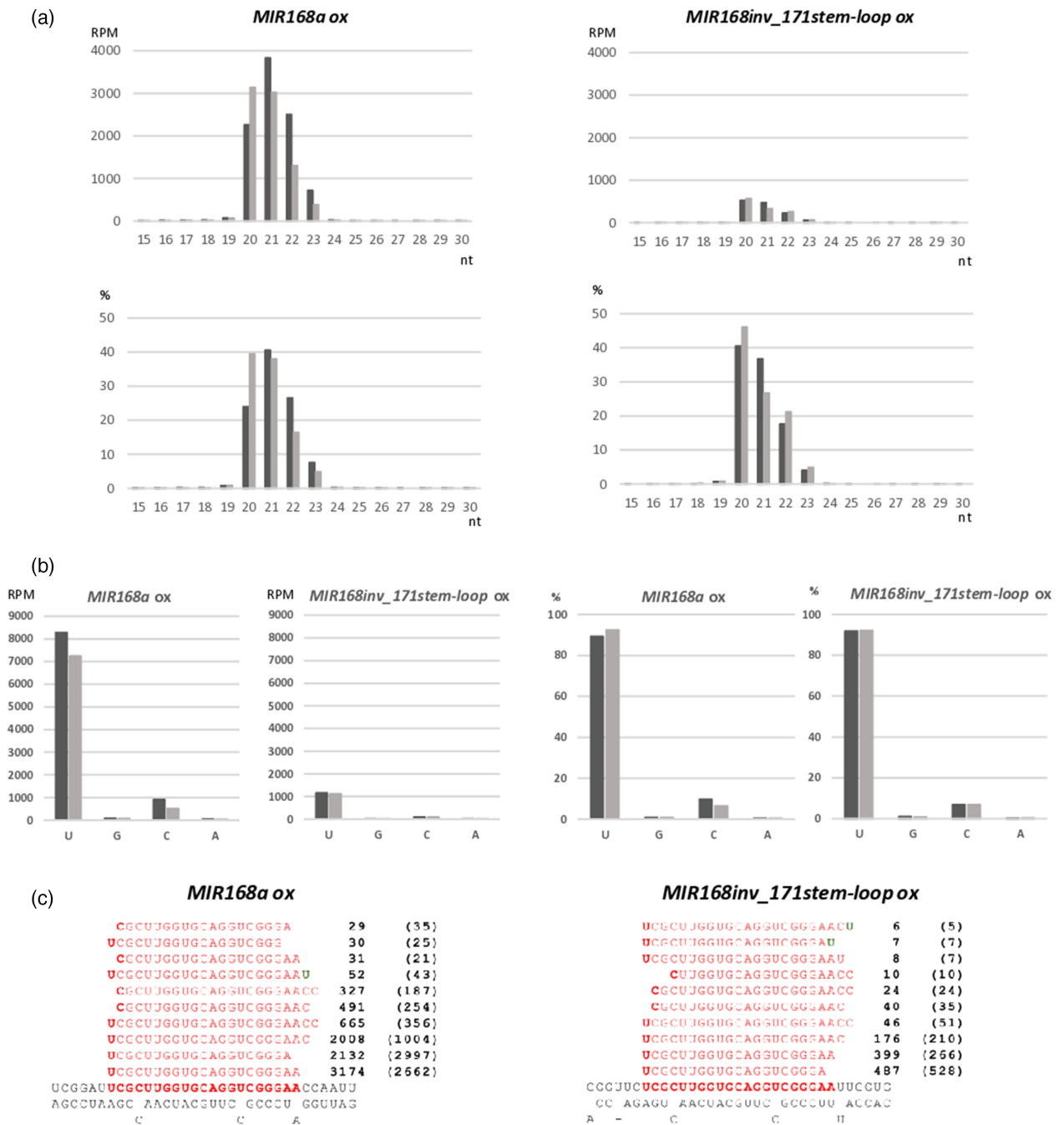


Figure 4. MiR168 iso-miR distribution in HTS data of *MIR168a* and *MIR168inv_171stem-loop* precursor fragment construct over-expressing transgenic plants. (a) Size distribution of the iso-miR168 reads in *MIR168a* and *MIR168inv_171stem-loop* over-expressor plants. The upper panels show read per million (RPM) values; the lower charts present percentages of the categories. Replica experiments were labeled with dark and light gray. (b) 5' End nucleotide distribution of reads mapped to the mature miRNA containing precursor strands. Left panels show read per million (RPM) values; the charts on the right present percentages of the categories. (c) RPM values of the 10 most abundant iso-miR168 sequences. RPM was calculated based on genome-mapped read number lacking nuclear, transfer, and ribosomal sRNAs. Numbers in brackets represent results of the replica experiments.

species were observed when the modified duplex was inserted into the *MIR168* backbone (*aMIR168*), reducing loading efficiency to 7% (Figure 5b). These findings

indicate the important role of distal precursor parts in determining AGO loading efficiency and also the cooperative action of various precursor elements.

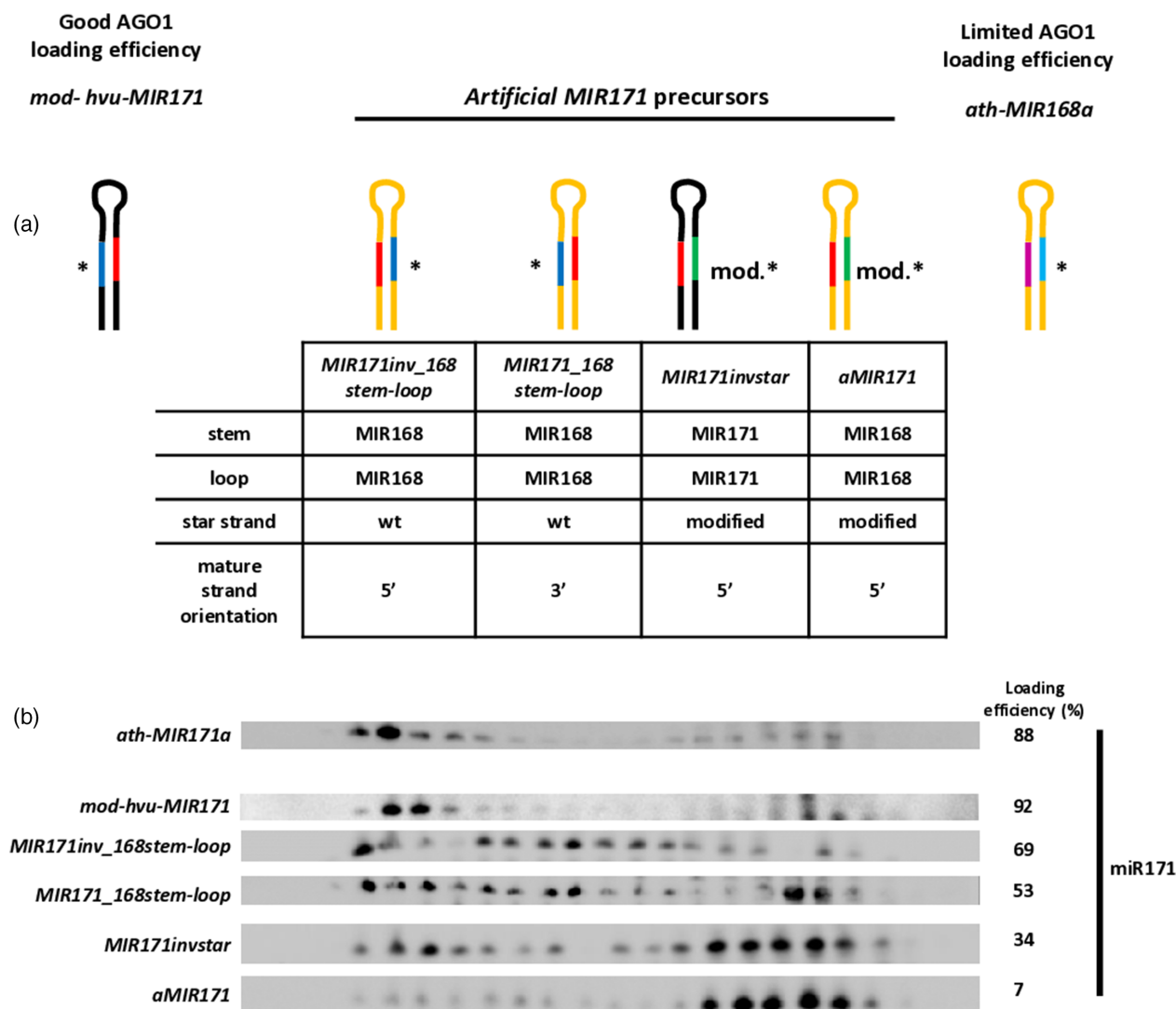


Figure 5. Composition of the chimeric and artificial miR171 producing precursor constructs and loading efficiency of the miR171 in the transient over-expression assays.

(a) Pink and red show mature miR168 and miR171, respectively; light blue and dark blue highlight the corresponding star strands. Green labels the modified miR171 star strand mimicking the miR168/miR168* duplex. Yellow and black lines represent the respective *ath-MIR168* and modified *hvu-MIR171* precursor parts. * the miR168 passenger strands within the constructs.

(b) Distribution of miR171 amongst the gel-filtration fractions prepared from the transient over-expression experiments of the indicated precursor constructs. For description of loading efficiency, see "Materials and Methods" section.

DISCUSSION

The auto-regulatory post-transcriptional control of AGO1 level involves the action of miR168 on *AGO1* mRNA. The production of miR168 is unique since it is extraordinarily resistant to mutations affecting genes playing important roles in miRNA biogenesis (Reis et al., 2015; Vaucheret et al., 2006). Recently, it was found that individual miRNAs can accumulate in both AGO-bound (HMW-RISC) and cytosolic AGO-unbound forms, classifying them into low, medium, and well-loading categories depending on their loading efficiency (bound/(bound + unbound) ratios) (Dalmadi et al., 2019). These experiments identified

miR168 as a low and miR171 as a better AGO-loading miRNA species, respectively. The superfluous generation and cytoplasmic sorting of miR168 species indicated a regulatory step at miR168 AGO-loading. Indeed, utilizing transient and transgenic over-expression assays, it was revealed that modification of the miR168* strand to turn the miR168/miR168* duplex structure into one similar to that of the miR171/miR171* duplex resulted in higher loading efficiency of the generated miR168 pool and enhanced AGO1 down-regulation (Dalmadi et al., 2021). These data showed that the structural elements of miRNA/miRNA* duplexes can convey signals influencing AGO-loading.

However, the question of whether the precursor structural/sequence elements, apart from the miRNA/miRNA* duplex region, can have any effect on AGO-loading efficiency remained unanswered (Figure 6).

Our current study dissects the contribution of the non-duplex parts of miRNA precursors to define AGO-loading efficiency. We have demonstrated by constructing a series of *MIR168/MIR171* chimeras that proximal (stem) and distal (loop) parts of the precursor can have impacts on AGO-loading efficiency to different extents. The mature miRNA strand of the miRNA/miRNA* duplex can be situated either on the 5' or on the 3' arm of the *MIRNA* precursor hairpin structure. The possibility that the 5' or 3' orientation of the miRNA strand may have altered effects on the miRNA AGO-loading abilities was raised initially based on the different representation of the two orientation types of miRNAs among the various loading efficiency categories. According to the previous study, the 3' originated miRNAs are over-represented in the well-loaded category (63% of the 3' matured miRNAs) compared to the low-loaded category (13%). Moreover, more 5' arm produced mature miRNA species accumulated in the low-loaded category (18 out of 22) than 3' originated (4 out of 22; Figure S14a,b) (Dalmadi et al., 2019). The well-loading type miR171 is located on the 3' arm while miR168 is produced from the 5' arm of the *MIRNA* precursor. By inversion of the orientation of the miR168/miR168* duplex, the mature miR168 strand was placed on the 3' arm in the modified *MIR168a* precursor (*MIR168inv*). This modification caused no significant alterations in the AGO-loading efficiency or in target down-regulation, indicating that miR168 orientation does not have a stand-alone role in modulation of the loading efficiency.

To assess the role of the remote parts of the precursor structure in AGO-loading efficiency of miR168 chimeric *MIR168/MIR171* precursor constructs containing either the loop or the stem parts of the *hvu-MIR171*, in combination with the 3' mature strand orientation, were created. The replacement of the loop section failed to initiate a remarkable change in the activity of the miR168 since the improvement of the loading and the target down-regulation was not significant. In contrast, changing the stem region, accompanied by the 3' miR168 orientation, proved to be more effective, significantly enhancing miR168 activity. The highest enhancement in miR168 AGO-loading and sensor target down-regulation was achieved in transient assays using the *MIR168inv_171stem-loop* construct, including both the stem and the loop regions of the *hvu-MIR171* precursor and the miR168/miR168* duplex in a 3' mature strand orientation. These findings indicate that not only the miR168/miR168* duplex but also other remote

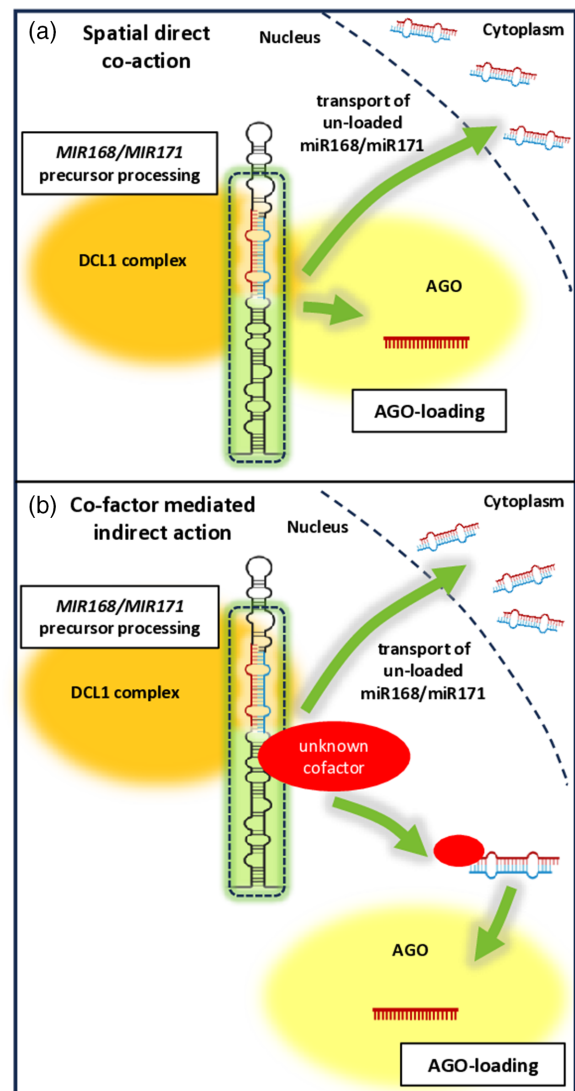


Figure 6. Possible models for the connection between the biogenesis and AGO loading of the investigated *MIR168/hvu-MIR171* precursors.

(a) miRNA biogenesis and AGO loading can spatially overlap in the vicinity of the chromatin during co-transcriptional processing of pri-miRNAs in the nucleus. The sites of miRNA biogenesis and AGO loading are marked by orange and yellow areas, respectively. The miR168/miR168* duplex is marked by red and blue lines. The information embodied in the stem part of the miRNA precursor structure, in cooperation with signals of the miRNA duplex (structural unit framed with dotted line), can directly modulate AGO-loading efficiency (short green arrow) of a subset of the generated miRNAs (red line) due to spatial proximity of the two processes. The non-loaded miRNA duplexes are sorted to cytoplasm (long green line with arrowhead).

(b) As an alternative scenario, yet unknown protein co-factor(s) (red oval) is/are attracted by structure/sequence information embodied in the stem part of the miRNA precursor in cooperation with the miRNA duplex section. This recruited co-factor could mark the miRNA/miRNA* duplex directly or indirectly by attaching to the duplex or mediating the attachment of another co-factor, indirectly modulating the loading efficiency of a subset of the miRNA pool into spatially separated, remote AGO proteins.

parts of the miRNA precursor structure, bordering the miRNA duplex, can have a significant impact on AGO1 loading. Intriguingly, the replacement of the stem and loop regions with the corresponding *hvu-MIR171* precursor sections alone was less effective in inducing higher AGO-loading and target down-regulation when the mature miR168 was situated in a 5' position of the duplex in the *MIR168_171stem-loop* construct. This observation supports the theory of cooperative actions between the investigated elements of the *MIRNA* precursor and highlights the importance of miRNA/miRNA* duplex orientation in combination with the other structural elements in relation to miRNA activity. The enhanced AGO-loading of miR168 produced from chimeric precursor containing the stem and loop structure of *hvu-MIR171* and the inversely orientated miR168/miR168* duplex was also confirmed in transgenic over-expression plant studies.

The specific sorting of different miRNAs into one of the 10 AGO proteins inherent in Arabidopsis cells depends highly on the identity of their 5' end nucleotide. Particularly, AGO1 as the main executor of the miRNA pathway loads predominantly miRNAs with uracil at their 5' terminus. In our previous work, using artificial *MIR168* precursor constructs having the complete backbone (both stem and loop regions) and miRNA duplex orientation and structure of *hvu-MIR171*, we confirmed the unaltered sorting of the produced miR168 (Dalmadi et al., 2021). In the case of this extensively modified precursor construct, high-throughput sequencing verified the processing of canonical miR168 species, which were sorted predominantly into AGO1. The HTS sequencing of the miRNA pool confirmed the unaltered processing of the *MIR168inv_171stem-loop* precursor construct and the production of canonical miR168 species with uracil at their 5' terminus. These results support the assumption that the sorting of the *MIR168inv_171stem-loop* originated miR168 did not change, and the observed phenotypical alterations and enhanced target down-regulation of the transgenic plants are due to the improved loading capacity of miR168. Indeed, gel-filtration experiments revealed the relatively higher presence of miR168-loaded HMW-RISCs in *MIR168inv_171stem-loop* plants and infiltrated leaves compared to wild-type *MIR168a* over-expressors, and immuno-precipitation identified the AGO1-loaded miR168 of *MIR168inv_171stem-loop* (Figure 2d; Figures S7c and 9).

The role of remote precursor elements in determining AGO-loading capacity of miRNAs was further investigated in transient studies, where wild type and modified miR171 duplexes were introduced into *MIR168a* backbone in various orientations (Figure 5). It was found that the *MIR168* backbone can limit the incorporation of miR171 into high molecular weight AGO-complexes, especially when the miR171 duplex orientation was inverted. In addition, it was also shown that reshaping of the miR171 duplex structure

similar to that of miR168 in *hvu-MIR171* backbone has a profound limitation effect on AGO-loading efficiency, as it was expected based on previous results (Dalmadi et al., 2021). However, the most inhibited AGO-loading was observed in the case when the modified miR171 duplex was introduced into the *MIR168a* backbone. These experiments indicate that the high AGO-loading capacity of miR171 can be converted into medium or low efficiencies by modulating the precursor components and also further support the cooperative action of various precursor elements.

The observation that precursor elements located outside of the miRNA/miRNA* duplex region can have an effect on the AGO-loading efficiency indicates that the transcription/processing of *MIRNA* precursors and AGO1 loading are coordinated and can trigger several important questions. To explain the regulatory action of remote miRNA precursor elements on AGO-loading, we can envision two scenarios involving direct or indirect connections between miRNA biogenesis and AGO-loading. As the first possibility, we propose a model where miRNA biogenesis and AGO1 loading spatially overlap in the vicinity of the chromatin. According to this scenario, the cooperative information coded mainly on the stem part of the miRNA precursor structure and in the miRNA duplex can directly convey information to AGO1 loading (Figure 5a). There are cumulating evidences showing that AGO1 activity can be spatially overlapping with sites of miRNA biogenesis. According to the traditional view of miRNA biogenesis in plants, *MIR* genes are transcribed by RNA Polymerase II (Pol II) then, pri-miRNAs are located in subnuclear speckles (Dicing body; D-body) where the release of imperfect miRNA/miRNA* duplexes is generated due to sequential cleavages of DCL1. Previously, it was thought that the miRNA loading of AGO1 exclusively occurs in the cytoplasm subsequently to the transport of the miRNA/miRNA* duplexes from the nucleus. However, recent results demonstrated the nucleo-cytoplasmic shuttling of AGO1 and proposed the nuclear loading of miRNAs followed by active transport of the complex back to the cytoplasm (Bologna et al., 2018; Zhang et al., 2020). This finding indicates that at least one of the main places of AGO1 loading resides in the nucleus bringing AGO1 in close vicinity to the site of miRNA production. Recent evidences also show that the processing of pri-miRNAs can be initiated during the transcription, leading to co-transcriptional production of plant miRNAs (Cambiagno et al., 2021; Gonzalo et al., 2022). In this model, at least the first DCL1 cleavage, depending on the processing type of the particular miRNA precursor, occurs on the pri-miRNA co-transcriptionally.

To assess the role of the processing type of various miRNAs in the determination of AGO-loading efficiency, we compared data sets presented about the types of processing (Bologna et al., 2013; Moro et al., 2018) and AGO-

loading efficiencies (Dalmadi et al., 2019) of Arabidopsis miRNAs. Based on the 30 miRNA families displayed in both datasets, we could not detect any connection between the type of processing and loading efficiencies of particular miRNAs, but further extensive experiments are needed to clarify whether there is any correlation between them. We found that miRNAs exhibiting loop-to-base processing show both low and high AGO-loading efficiencies, like *MIR156* and *MIR319*, respectively. In addition, *MIR159a*, which also possesses a loop-to-base processing type (Bologna et al., 2009), produces a very efficiently loaded miRNA. A similar phenomenon can be observed in the case of miRNAs processed by base-to-loop manner; *MIR168a* produces low, *MIR167* intermediate, while *MIR171a* efficiently loaded miRNAs. The loading properties of miRNAs matured from *MIR159a*, *MIR168a*, and *MIR171a* were investigated also in transient and stable transgenic over-expression studies, confirming that loading abilities of miRNAs do not change due to high levels of over-expression. These data suggest that the processing type of particular miRNAs may not have a major role in determining AGO-loading efficiencies (Figure S14c). *Hvu-MIR171* was selected by its ability to produce efficiently loaded miRNA onto high molecular weight AGO-complexes and the practical technical properties based on previous work (Kis et al., 2016). However, we do not have experimental data about the processing type of this miRNA. Hence, we cannot exclude the possibility that modifications in the chimeric precursors can alter to some extent the processing type of the particular artificial miRNA precursor, which in turn might interfere with AGO-loading capacity. Further experiments will be necessary to clarify this issue.

The potential co-localization of AGO1 and miRNA biogenesis (Figure 6a) is supported by recent findings revealing the various functions of AGO1 in association with the chromatin. AGO1 can bind to the chromatin of active genes and modulate their expression in response to various stimuli (Liu et al., 2018). Moreover, under stress conditions, miR161 and miR173 were stabilized in the cytoplasm while the expressions of their *MIR161* and *MIR173* pri-miRNAs by Pol II were negatively regulated in the nucleus, both in AGO1 dependent manner (Dolata et al., 2016). Recent data showed that AGO1 associates with *COOLAIR* and also with subunits of Pol II, playing a role in the control of flowering (Nazer & Kornblihtt, 2021). There was also a protein factor, *REDUCTION IN BLEACHED VEIN AREA* (RBV), identified with dual action in promoting both the pri-miRNA transcription and the AGO1-loading of miRNAs (Liang et al., 2022). These evidences point out that AGO1 can also be found in the vicinity of chromatin, playing various regulatory roles, rendering the spatial connection of AGO1 loading and miRNA biogenesis probable.

An alternative scenario is also possible where the processing of the investigated precursors and the loading of

the produced miR168 or miR171 has an indirect connection (Figure 6b). This model implies that protein co-factor(s) is/are attracted by structure/sequence information embodied in the stem part of the miRNA precursor and the duplex region. The recruited co-factor(s) could mark the miRNA/miRNA* duplex directly or indirectly by attaching to the duplex or mediating the attachment of another co-factor, which modulates the loading of the miRNA into the remote AGO1 protein (Figure 5b). In line with this hypothesis, it was shown that miRNA processing is dependent on accessory proteins, such as *HYPONASTIC LEAVES 1* (HYL1) and *SERRATE* (SE) (Ding & Zhang, 2023; Mencia et al., 2023). It was suggested that HYL1 can be linked to the generated miRNA/miRNA* duplexes and subsequently these complexes are also associated with *CONSTITUTIVE ALTERATIONS IN THE SMALL RNAS PATHWAYS 9* (CARP9) (Tomassi et al., 2020). CARP9 is recruited to the complex by the interaction with HYL1 and in the nucleus AGO1 can associate with the complex through the interaction of CARP9 with the HSP90-mediated AGO1 loading. Moreover, it was also demonstrated that the members of the *DOUBLE-STRANDED RNA BINDING* (DRB) protein family can both be components of miRNA biogenesis and take part in the target down-regulation either with the coordination of the cleavage (HYL1/DRB1) or the translational inhibition (DRB2) of the target mRNA (Eamens, Kim, et al., 2012; Eamens, Wook Kim, & Waterhouse, 2012). *HASTY* (HST), another important player of miRNA biogenesis, can act as a scaffold protein facilitating complex formation between DCL1 and MED37 at *MIRNA* genes promoting pri-miRNA processing/transcription (Cambiagno et al., 2021). The loading of miRNAs into AGO1 is also affected by protein co-factors; *TRANSPORTIN1* (TRN1) enhances miRNA activity by promoting miRNA-AGO1 association (Cui et al., 2016) while *ENHANCED MiRNA ACTIVITY1* (EMA1) negatively regulates the loading of miRNAs into AGO1 (Wang et al., 2011). These findings show that protein co-factors can bind directly to the miRNA duplexes or indirectly modulate the activity of miRNAs. Based on these data, it is possible that a known or a still unknown protein co-factor can recognize remote signals on the precursors presented in this work and modulate the action of the generated miRNA.

In contrast to the miRNA/miRNA* duplexes, which directly interact with AGO proteins explaining the effects of their structural signals on AGO loading and sorting, the precursor elements flanking miRNA duplexes (stem and loop structures) were thought to be spatially separated from the sites of AGO loading. However, the regulatory action of these remote structural/sequence signals suggests that at least a subset of the miRNA biogenesis and the AGO loading are spatially overlapping or these remote signals have the capacity to mark these miRNA duplexes for downstream processes and modulate AGO loading

spatially separated from miRNA biogenesis. Since plant miRNA precursors are extremely variable in size and structure, it is expected that these structures/sequences include further signals influencing the processing, maturation, sorting, and loading of miRNAs possibly in response to developmental and environmental cues. However, to test how universal this effect of remote precursor elements on loading efficiency is, investigation of other miRNAs is needed.

MATERIALS AND METHODS

Plant material and growth conditions

Arabidopsis thaliana seeds were surface sterilized and after incubation for 3 days at 4°C, transgenic and wild-type Columbia plants were germinated at 21°C on MS agar medium supplied with 1% sucrose with or without the presence of 50 µg ml⁻¹ kanamycin, respectively. Seedlings were transferred into Jiffy peat blocks after 7 days, and spent 4 weeks there before planting in pots filled with soil. Plants were grown under 8 h light/16 h dark cycles at 21°C until planting, and then were moved to a light room under 16 h light/8 h dark at 21°C. *Nicotiana benthamiana* plants were grown under the light room conditions described above.

Plasmid construction

All constructs were built using the pGreen binary vector system (John Innes Center, Norwich, UK; pGreen0029) and 35S cassette according to the instructions of the manufacturer (<http://www.pgreen.ac.uk>). We used the previously described *MIR168a* precursor construct containing the region 10–10 bp upstream and downstream from the position of the miRNA stem-loop structure (Dalmadi et al., 2019) and *hvu-MIR171* described previously (Kis et al., 2016; <https://www.mirbase.org/results/?query=hvu-miR171>). *MIR171inv_168stem-loop*, *aMIR171*, and *MIR171_168stem-loop* were created with the PCR mutagenesis of *MIR168a*. *MIR168inv_171stem-loop*, *MIR168_171stem-loop*, and *MIR171inv-star* were produced with the PCR mutagenesis of the modified *hvu-MIR171*. *MIR168inv*, *MIR168inv_171loop*, and *MIR168inv_171stem* were synthesized as gBlocks (IDT, Coralville, Iowa, USA) fragments and were used for cloning directly into the 35S cassette of the pGreen system. For the *AGO1-sensor*, the same construct was used as previously described (Dalmadi et al., 2021), which consists of the 558-bp-long cDNA fragment containing the miR168 target site fused to the 5' part of GFP in-frame. Oligonucleotides used to create constructs were presented in Table S4. All constructs were introduced into *Agrobacterium tumefaciens* AGL1 strain with electroporation (360 Ω, 25 µF, 2.5 kV; Bio-Rad, Hercules, California, USA) in the presence of the pSoup helper plasmid.

Transient assay

Young leaves of 6 weeks old *N. benthamiana* were infiltrated with the respective mixture of *Agrobacterium tumefaciens* (AGL1) suspensions at 1.0 optical density of 600 nm [OD₆₀₀] containing sensor, miRNA-producing, and P14 constructs as described previously (Dalmadi et al., 2021). P14, as a suppressor of the siRNA pathway, was included in every experiment with a uniform concentration (Szádeczky-Kardoss et al., 2018), so it did not interfere with the observation of relative signal reduction. To reduce the differences in miRNA production ability of the different constructs, normalized

amounts were applied, and mixtures were supplemented with the empty pGreen0029 vector containing *A. tumefaciens* (AGL1). For a detailed compilation of infiltration mixtures, see Table S1. Samples were taken on the third day post-infiltration; four discs of 1 cm diameter were pooled from patches of separate leaves for individual constructs. Samples were collected in parallel from both sides of the same leaves. Every miRNA-producing sensor construct combination was tested on four to five plants, and each experiment was repeated at least three times.

For FPLC experiments, 0.3 g of fully infiltrated leaves were collected.

Two experimental setups were used: one includes also the infiltration of a mixture containing *pGreen0029* empty vector instead of the miR168 producer construct as a negative control and one involving only wild-type *MIR168a* and a respective modified precursor construct (Figure 2; Figures S2–S6).

Transgenic line production

Arabidopsis thaliana Columbia ecotype plants were transformed with the appropriate miR168 producing construct according to the standard floral dip protocol (Davis et al., 2009). Transformant T0 plants were selected on MS plates supplemented with 50 µg ml⁻¹ kanamycin. Four weeks after planting, their miR168 expression profile in young rosette leaves was analyzed, and plants exhibiting an appropriate miR168 over-expression level were self-pollinated and used to generate transgenic lines. Homozygous lines were produced with self-pollination during two further generations. Selection was based on kanamycin resistance and a consistent level of miR168 expression. To demonstrate the effect of over-expression, lines with the most comparable expression level were selected, having an over-expression rate compared with *Columbia* wild-type between 3- and 12-fold.

Gel-filtration assay

Gel-filtration based size separation of crude extracts using Superdex-200 column was performed as described previously (Lakatos et al., 2004; Várallyay et al., 2010) with minor modifications. In the case of Figure S9, 48 fractions of gel-filtration were divided into two and RNA was extracted with the phenol-chloroform method from the odd samples, while even samples were used for protein purification using acetone precipitation. In other cases, all the fractions were used to produce RNA samples. Crude extracts were prepared from 0.3 g plant material collected from leaves of *N. benthamiana* plants 3 days post-infiltration (Figures 2d and 5b; Figure S7) and from 7-day-old *Arabidopsis* seedlings (Figure S9a). In the case of a given panel, all samples were collected in parallel and gel-filtration runs were carried out subsequently with the same parameters.

RNA extraction and protein sample preparation

For miRNA and protein analyses, indicated quantities of agro-infiltrated leaves (Figure 2b; Figures S2–S6) or 0.1–0.2 g of *A. thaliana* rosette leaves (Figure 3b; Figure S8b) were collected, homogenized in an ice-cold mortar in 355 µl of extraction buffer (0.1 M glycine-NaOH, pH 9.0, 100 mM NaCl, 10 mM EDTA, 2% sodium dodecyl sulfate, and 1% sodium lauroylsarcosine) and divided into two aliquots. To one part (60 µl) an equal amount of 2 × Laemmli buffer was added and centrifuged for 5 min after boiling for 5 min. The remaining part was supplemented with 355 µl extraction buffer and used for RNA extraction with the standard phenol-chloroform method. This method ensures the comparability of protein and RNA samples within one panel.

miRNA detection and quantification

For small RNA northern blot analyses, 4 µg of total RNA or samples of gel-filtration were fractionated on denaturing 12% polyacrylamide gels containing 8 M urea and transferred to Hybond NX membrane (GE Healthcare, Chicago, Illinois, USA) with semi-dry blotting (Bio-Rad, Hercules, California, USA). Membranes were chemically cross-linked (Pall & Hamilton, 2008) and probed with either locked nucleic acid (LNA) oligonucleotide probes (Exiqon, Vedbaek, Denmark) (Figure S7c) or DNA probes, both biotinylated at the 5' end. Signal was detected using Chemiluminescent Nucleic Acid Detection Module (ThermoFischer, Waltham, MA, USA; Cat. Kit: 89880) and images were acquired with ChemiDoc equipment in Chemi High Resolution mode. For the analysis of gel-filtration blots, volume intensity of the three most prominent RISC loaded and unbound fractions was measured and summarized. Loading efficiency was calculated as RISC-loaded volume intensity divided by the total sum of RISC loaded plus unbound volume intensities and was represented as a percentage (Figures 2d and 5b; Figure S7c). To calculate relative loading efficiency, the loading efficiency was referred to the protein level of the sample (Figure S9). Within one panel, images of different miRNAs were produced with subsequent probing of the same membrane after washing. Over-expression rate of miR168 in transgenic plants was determined based on volume intensity normalized to the corresponding U6 signal.

Western blotting

A total of 8 µl extract of infiltrated *N. benthamiana* leaves, or 20 µl of Arabidopsis samples, were separated on 8% sodium dodecylsulphate-polyacrylamide gel, blotted overnight to PVDF Transfer Membrane (Hybond-P; GE Healthcare Freiburg, Germany) using wet tank transfer, and subjected to western blot analysis. Membranes were blocked using 5% non-fat dry milk in phosphate-buffered saline (PBS) containing 0.05% Tween 20 (PBST) for 60 min. Blots were cut into two, and respective parts were incubated with anti-BiP (Agrisera, Vannas, Sweden; AS09 481) for 1 h or with anti-AGO1 (Agrisera; AS09 527) for 2.5 h at a dilution of 1:7500 in 1% non-fat dried milk in 1 × PBST. After washing in PBST, the blot was incubated with secondary goat anti-rabbit IgG HRP conjugated antibody (Agrisera; AS09 602) for 1 h at a dilution of 1:10 000 in 1 × PBST with agitation. Blots were developed with High Clarity Western ECL (Bio-Rad); exposure was made using ChemiDoc (Bio-Rad) equipment in signal accumulation mode. Volume intensity of AGO1 signal was normalized to BiP; relative accumulation was presented based on Columbia wild-type or the respective *MIR168a* precursor over-expressing sample. AGO1-sensor was detected with anti-AGO1 antibody.

High-throughput sequencing (HTS)

To create cDNA libraries for sequencing, high-quality RNA samples were purified with the phenol-chloroform method from 0.3 g of bulked seedlings of respective homozygote lines. About 20 µg of the samples were loaded onto separate polyacrylamide gels, the small RNA fraction was isolated and libraries were prepared only from this fraction using the Truseq Small RNA Library Preparation Kit (Illumina, San Diego, CA, USA) and the modified protocol described earlier (Czotter et al., 2018). Sequencing was carried out on HiScanSQ by UD-Genomed (Debrecen, Hungary) with a 50 bp, single-end chemistry (8 samples/sequencing lane). QIAGEN CLC Genomics Workbench (Hilden, Germany) 20 was used for sequence analysis. First, raw sequences were subjected to quality control, adapters and stop sequences were trimmed and reads within the

15–30 nucleotide size range were used for further analysis. Reads mapped to the Arabidopsis genome were then filtered for ribosomal or tRNA originated and small nuclear and nucleolar RNAs. These filtered read numbers of different libraries varied between 2.7 and 5.7 million, and reads per million (RPM) were calculated on these bases respectively for every data row. Following, these reads were mapped to the wild-type *ath-pri-MIR168a*, *ath-pri-MIR168b*, and to the *MIR168inv_171stem-loop* modified precursor sequence, respectively, using the Map Reads to Reference tool. The created alignments were extracted to new sequence lists, and with the help of Microarray and Small RNA Analysis tool of CLC Genomics Workbench, reads of individual sequences were counted and exported to a single Excel file. The selected complementary reads were used for further analysis. For the analysis of AGO1-derived siRNAs, the whole cDNA sequence of *ath-AGO1* mRNA was used as reference.

Immuno-precipitation

For crude extracts, 0.4 g of seedlings was homogenized in four volumes of lysis buffer (10 mM Tris-HCl pH 7.6; 1 mM EDTA; 150 mM NaCl; 10% glycerol; 0.5% Nonidet P-40; 5 mM NaF; 1 mM dithiothreitol; 0.5 mM Na₂VO₄; 1 mM phenylmethylsulfonyl fluoride), and centrifuged three times at 4°C in fresh tubes to get rid of cellular debris. As an input sample, 100 µl of extracts were used to purify RNA with the phenol-chloroform method and protein by adding an equal volume of Laemmli buffer (2×). RNA was dissolved in 20 µl nuclease-free water. About 1 ml extract was pre-incubated with 3 µl anti-AGO1 HRP-conjugated antibody (Agrisera) for 2 h at 4°C with agitation, then applied to Dynabeads Kit (Thermo Fisher Scientific) according to the manufacturer. Immuno-precipitated fraction was eluted in 20 µl, from which 10 µl was used to purify RNA. To the remaining 10 µl, an equal volume of Laemmli buffer was added and used as a protein sample. Input RNA samples for northern blot were diluted 40 times before loading, and the same volume of input and immuno-precipitated samples were applied on the gel. Northern and western blots were carried out as described above. Volume intensities of miR168 blots were measured with ImageLab 5.2.1 software of ChemiDoc equipment (Bio-Rad). MiR168 signal volume intensities of immuno-precipitated samples were referred to input sample volume intensity and AGO1 level in corresponding IP samples. Relative fold changes (RFC on figures) were presented relative to *MIR168a* line (Figure S9b).

ACCESSION NUMBERS

Raw data from the RNA have been deposited in the NCBI BioProject database under the ID PRJNA1090017.

AUTHOR CONTRIBUTIONS

ÁD and ZH: conceptualization; FM: data curation; ZH and AK: funding acquisition; ÁD, FM, and AA: investigation; ÁD: methodology; ÁD, ZH, and AK: project administration; ZH and AK: resources; FM: software; ÁD: validation; ÁD and ZH: supervision; ÁD and ZH: writing – original draft; ÁD and ZH: writing – review and editing.

ACKNOWLEDGMENTS

We thank Erzsébet Poldán for her valuable assistance in the laboratory. This work was supported by the Hungarian Research, Development and Innovation Office (NKFIH), grant numbers K125300 and K134914, and the Hungarian Academy of Sciences, Hungarian National Laboratory Program, grant number RRF-2.3.1-21-2022-00007. This work was supported by the Flagship Research

group Program of the Hungarian University of Agriculture and Life Sciences.

CONFLICT OF INTEREST

The authors declare no competing interests.

DATA AVAILABILITY STATEMENT

Raw data from the RNA have been deposited in the NCBI BioProject database under the ID PRJNA1090017.

SUPPORTING INFORMATION

Additional Supporting Information may be found in the online version of this article.

Figure S1. Sequence and the predicted structure of the used miR168 producing precursor hairpins.

Figure S2. Replica experiments for transient assay of *MIR168a* and *MIR168inv*.

Figure S3. Replica experiments for transient assay of *MIR168a* and *MIR168inv_171loop*.

Figure S4. Replica experiments for transient assay of *MIR168a* and *MIR168inv_171stem*.

Figure S5. Replica experiments for transient assay of *MIR168a* and *MIR168inv_171stem-loop*.

Figure S6. Replica experiments for transient assay of *MIR168a* and *MIR168_171stem-loop*.

Figure S7. Detection of the functional high molecular weight RISC in our experimental setup and replica gel-filtrations.

Figure S8. Phenotypical appearance, miR168 and AGO1 content of transgenic lines.

Figure S9. Gel-filtration experiments of the transgenic plants.

Figure S10: Size distribution of miR168 iso-forms in total RNA of *Arabidopsis thaliana* flowers and in AGO1-associated sequencing data.

Figure S11. Abundance of 20–24 nt long *Ago1* originated siRNAs in HTS data.

Figure S12. Sequence and the predicted structure of the used miR171 producing precursor hairpins.

Figure S13. Original images of miR171 northern blots prepared from the FPLC fractions of ath-miR171a, mod-hvu-MIR171, MIR171-inv_168stem-loop, MIR171_168 stem-loop, MIR171invstar, and aMIR171 construct over-expression. Gel-filtration fractions used in calculations as AGO1 containing High Molecular Weight RISC (HMW-RISC) and AGO-unbound sRNAs are indicated with rectangles. Arrows show the AGO-loading competent 21 nt miR171. Right brace labels the detected AGO-incompetent sRNAs.

Figure S14. Distribution of 3' and 5' miRNAs amongst the loading type groups.

Table S1. Composition of the *Agrobacterium* mixtures used in the infiltration experiments.

Table S2. Statistical evaluation of AGO1-sensor datasets gained from transient expression experiments.

Table S3. Normalized read number of the passenger strand iso-forms in the HTS data.

Table S4. List of oligonucleotides used to produce the constructs.

REFERENCES

Addo-Quaye, C., Snyder, J.A., Park, Y.B., Li, Y.F., Sunkar, R. & Axtell, M.J. (2009) Sliced microRNA targets and precise loop-first processing

of hairpins revealed by analysis of the degradome. *RNA*, **15**, 2112–2121.

Axtell, M.J., Westholm, J.O. & Lai, E.C. (2011) Vive la difference: biogenesis and evolution of microRNAs in plants and animals. *Genome Biology*, **12**, 221.

Bologna, N.G., Iselin, R., Abriata, L.A., Sarazin, A., Pumplin, N., Jay, F. *et al.* (2018) Nucleo-cytosolic shuttling of ARGONAUTE1 prompts a revised model of the plant microRNA pathway. *Molecular Cell*, **69**, 709–719.e5.

Bologna, N.G., Mateos, J.L., Bresso, E.G. & Palatnik, J.F. (2009) A loop-to-base processing mechanism underlies the biogenesis of plant microRNAs miR319 and miR159. *The EMBO Journal*, **28**, 3646–3656.

Bologna, N.G., Schapire, A.L., Zhai, J.X., Chorostecki, U., Boissbouvier, J., Meyers, B.C. *et al.* (2013) Multiple RNA recognition patterns during microRNA biogenesis in plants. *Genome Research*, **23**, 1675–1689.

Cambiagno, D.A., Giudicatti, A.J., Arce, A.L., Gagliardi, D., Li, L., Yuan, W. *et al.* (2021) HASTY modulates miRNA biogenesis by linking pri-miRNA transcription and processing. *Molecular Plant*, **14**, 426–439.

Carrington, J.C. & Ambros, V. (2003) Role of microRNAs in plant and animal development. *Science*, **301**, 336–338.

Cui, Y.W., Fang, X.F. & Qi, Y.J. (2016) TRANSPORTIN1 promotes the association of microRNA with ARGONAUTE1 in Arabidopsis. *Plant Cell*, **28**, 2576–2585.

Czotter, N., Molnár, J., Pesti, R., Demián, E., Baráth, D., Varga, T. *et al.* (2018) Use of siRNAs for diagnosis of viruses associated to woody plants in nurseries and stock collections. *Methods in Molecular Biology*, **1746**, 115–130.

Dalmadi, A., Gyula, P., Bálint, J., Szittyá, G. & Havelda, Z. (2019) AGO-unbound cytosolic pool of mature miRNAs in plant cells reveals a novel regulatory step at AGO1 loading. *Nucleic Acids Research*, **47**, 9803–9817.

Dalmadi, A., Miloro, F., Bálint, J., Várallyay, É. & Havelda, Z. (2021) Controlled RISC loading efficiency of miR168 defined by miRNA duplex structure adjusts ARGONAUTE1 homeostasis. *Nucleic Acids Research*, **49**, 12912–12928.

Davis, A.M., Hall, A., Millar, A.J., Darrah, C. & Davis, S.J. (2009) Protocol: streamlined sub-protocols for floral-dip transformation and selection of transformants in *Arabidopsis thaliana*. *Plant Methods*, **5**, 3.

Ding, N. & Zhang, B.L. (2023) microRNA production in Arabidopsis. *Frontiers in Plant Science*, **14**, 1096772.

Dolata, J., Bajczyk, M., Bielewicz, D., Niedojadlo, K., Niedojadlo, J., Pietrykowska, H. *et al.* (2016) Salt stress reveals a new role for ARGONAUTE1 in miRNA biogenesis at the transcriptional and posttranscriptional levels. *Plant Physiology*, **172**, 297–312.

Dong, Q.K., Hu, B.B. & Zhang, C. (2022) microRNAs and their roles in plant development. *Frontiers in Plant Science*, **13**, 824240.

Eamens, A.L., Kim, K.W., Curtin, S.J. & Waterhouse, P.M. (2012) DRB2 is required for microRNA biogenesis in *Arabidopsis thaliana*. *PLoS One*, **7**, e35933.

Eamens, A.L., Smith, N.A., Curtin, S.J., Wang, M.B. & Waterhouse, P.M. (2009) The double-stranded RNA binding protein DRB1 directs guide strand selection from microRNA duplexes. *RNA*, **15**, 2219–2235.

Eamens, A.L., Wook Kim, K. & Waterhouse, P.M. (2012) DRB2, DRB3 and DRB5 function in a non-canonical microRNA pathway in *Arabidopsis thaliana*. *Plant Signaling & Behavior*, **7**, 1224–1229.

Endo, Y., Iwakawa, H.O. & Tomari, Y. (2013) ARGONAUTE7 selects miR390 through multiple checkpoints during RISC assembly. *EMBO Reports*, **14**, 652–658.

Gonzalo, L., Tossolini, I., Gulanicz, T., Cambiagno, D.A., Kasprowicz-Maluski, A., Smolinski, D.J. *et al.* (2022) R-loops at microRNA encoding loci promote co-transcriptional processing of pri-miRNAs in plants. *Nature Plants*, **8**, 402–418.

Hacquard, T., Clavel, M., Baldrich, P., Lechner, E., Perez-Salame, I., Scheptilnikov, M. *et al.* (2022) The Arabidopsis F-box protein FBW2 targets AGO1 for degradation to prevent spurious loading of illegitimate small RNA. *Cell Reports*, **39**, 110671.

Iki, T. (2017) Messages on small RNA duplexes in plants. *Journal of Plant Research*, **130**, 7–16.

Iki, T., Cléry, A., Bologna, N.G., Sarazin, A., Brosnan, C.A., Pumplin, N. *et al.* (2018) Structural flexibility enables alternative maturation, ARGONAUTE sorting and activities of miR168, a global gene silencing regulator in plants. *Molecular Plant*, **11**, 1008–1023.

- Kis, A., Tholt, G., Ivanics, M., Várallyay, E., Jenés, B. & Havelda, Z. (2016) Polycistronic artificial miRNA-mediated resistance to wheat dwarf virus in barley is highly efficient at low temperature. *Molecular Plant Pathology*, **17**, 427–437.
- Lakatos, L., Szittyá, G., Silhavy, D. & Burgyán, J. (2004) Molecular mechanism of RNA silencing suppression mediated by p19 protein of tombusviruses. *The EMBO Journal*, **23**, 876–884.
- Li, M. & Yu, B. (2021) Recent advances in the regulation of plant miRNA biogenesis. *RNA Biology*, **18**, 2087–2096.
- Liang, C., Cai, Q., Wang, F., Li, S.F., You, C.J., Xu, C. *et al.* (2022) RBV is a conserved WD40 repeat protein that promotes microRNA biogenesis and ARGONAUTE1 loading. *Nature Communications*, **13**, 1217.
- Liu, C., Xin, Y., Xu, L., Cai, Z.K., Xue, Y.C., Liu, Y. *et al.* (2018) ARGONAUTE 1 binds chromatin to promote gene transcription in response to hormones and stresses. *Developmental Cell*, **44**, 348.
- Mallory, A. & Vaucheret, H. (2010) Form, function, and regulation of ARGONAUTE proteins. *Plant Cell*, **22**, 3879–3889.
- Mateos, J.L., Bologna, N.G., Chorostecki, U. & Palatnik, J.F. (2010) Identification of MicroRNA processing determinants by random mutagenesis of Arabidopsis MIR172a precursor. *Current Biology*, **20**, 49–54.
- Mencia, R., Gonzalo, L., Tossolini, I., Manavella, P.A. & Ort, D. (2023) Keeping up with the miRNAs: current paradigms of the biogenesis pathway. *Journal of Experimental Botany*, **74**, 2213–2227.
- Mi, S.J., Cai, T., Hu, Y.G., Chen, Y., Hodges, E., Ni, F.R. *et al.* (2008) Sorting of small RNAs into Arabidopsis argonaute complexes is directed by the 5' terminal nucleotide. *Cell*, **133**, 116–127.
- Morel, J.B., Godon, C., Mourrain, P., Béclin, C., Boutet, S., Feuerbach, F. *et al.* (2002) Fertile hypomorphic ARGONAUTE (ago1) mutants impaired in post-transcriptional gene silencing and virus resistance. *Plant Cell*, **14**, 629–639.
- Moro, B., Chorostecki, U., Arikiti, S., Suarez, I.P., Höbartner, C., Rasia, R.M. *et al.* (2018) Efficiency and precision of microRNA biogenesis modes in plants. *Nucleic Acids Research*, **46**, 10709–10723.
- Narjala, A., Nair, A., Tirumalai, V., Sundar, G.V.H. & Shivaprasad, P.V. (2020) A conserved sequence signature is essential for robust plant miRNA biogenesis. *Nucleic Acids Research*, **48**, 3103–3118.
- Nazer, E. & Kornblihtt, A.R. (2021) Nuclear roles for argonaute proteins in the control of flowering. *Proceedings of the National Academy of Sciences of the United States of America*, **118**(52), e2120124118. Available from: <https://doi.org/10.1073/pnas.2120124118>
- Pall, G.S. & Hamilton, A.J. (2008) Improved northern blot method for enhanced detection of small RNA. *Nature Protocols*, **3**, 1077–1084.
- Reis, R.S., Hart-Smith, G., Eamens, A.L., Wilkins, M.R. & Waterhouse, P.M. (2015) Gene regulation by translational inhibition is determined by dicer partnering proteins. *Nature Plants*, **1**, 14027.
- Rojas, A.M.L., Drusin, S.I., Chorostecki, U., Mateos, J.L., Moro, B., Bologna, N.G. *et al.* (2020) Identification of key sequence features required for microRNA biogenesis in plants. *Nature Communications*, **11**, 5320.
- Song, L., Axtell, M.J. & Fedoroff, N.V. (2010) RNA secondary structural determinants of miRNA precursor processing in Arabidopsis. *Current Biology*, **20**, 37–41.
- Sunkar, R., Li, Y.F. & Jagadeeswaran, G. (2012) Functions of microRNAs in plant stress responses. *Trends in Plant Science*, **17**, 196–203.
- Szadeczyk-Kardoss, I., Csorba, T., Auber, A., Schamberger, A., Nyikó, T., Taller, J. *et al.* (2018) The nonstop decay and the RNA silencing systems operate cooperatively in plants. *Nucleic Acids Research*, **46**, 4632–4648.
- Takeda, A., Iwasaki, S., Watanabe, T., Utsumi, M. & Watanabe, Y. (2008) The mechanism selecting the guide strand from small RNA duplexes is different among argonaute proteins. *Plant & Cell Physiology*, **49**, 493–500.
- Tomassi, A.H., Re, D.A., Romani, F., Cambiagno, D.A., Gonzalo, L., Moreno, J.E. *et al.* (2020) The intrinsically disordered protein CARP9 bridges HYL1 to AGO1 in the nucleus to promote microRNA activity. *Plant Physiology*, **184**, 316–329.
- Várallyay, E., Válóci, A., Agyi, A., Burgyán, J. & Havelda, Z. (2010) Plant virus-mediated induction of miR168 is associated with repression of ARGONAUTE1 accumulation. *The EMBO Journal*, **29**, 3507–3519.
- Vaucheret, H., Mallory, A.C. & Bartel, D.P. (2006) AGO1 homeostasis entails coexpression of MIR168 and AGO1 and preferential stabilization of miR168 by AGO1. *Molecular Cell*, **22**, 129–136.
- Wang, W., Ye, R.Q., Xin, Y., Fang, X.F., Li, C.L., Shi, H.Q. *et al.* (2011) An importin β protein negatively regulates microRNA activity in Arabidopsis. *Plant Cell*, **23**, 3565–3576.
- Werner, S., Wollmann, H., Schneeberger, K. & Weigel, D. (2010) Structure determinants for accurate processing of miR172a in *Arabidopsis thaliana*. *Current Biology*, **20**, 42–48.
- Xu, Y. & Chen, X.M. (2023) microRNA biogenesis and stabilization in plants. *Fundamental Research*, **3**, 707–717.
- Zhang, B.L., You, C.J., Zhang, Y., Zeng, L.P., Hu, J., Zhao, M.L. *et al.* (2020) Linking key steps of microRNA biogenesis by TREX-2 and the nuclear pore complex in Arabidopsis. *Nature Plants*, **6**, 957.
- Zhang, X.M., Niu, D.D., Carbonell, A., Wang, A.R., Lee, A., Tun, V. *et al.* (2014) ARGONAUTE PIWI domain and microRNA duplex structure regulate small RNA sorting in Arabidopsis. *Nature Communications*, **5**, 5468.
- Zhu, H.L., Hu, F.Q., Wang, R.H., Zhou, X., Sze, S.H., Liou, L.W. *et al.* (2011) Argonaute10 specifically sequesters miR166/165 to regulate shoot apical meristem development. *Cell*, **145**, 242–256.
- Zhu, H.L., Zhou, Y.Y., Castillo-González, C., Lu, A., Ge, C.X., Zhao, Y.T. *et al.* (2013) Bi-directional processing of pri-miRNAs with branched terminal loops by Arabidopsis Dicer-like1. *Nature Structural & Molecular Biology*, **20**, 1106.